Cation distribution in nanocrystalline $ZnFe_2O_4$ investigated using x-ray absorption fine structure spectroscopy

2009 J. Phys.: Condens. Matter 21 405303

(http://iopscience.iop.org/0953-8984/21/40/405303)

J. Phys.: Condens. Matter **21** (2009) 405303 (9pp) doi:10.1088/0953-8984/21/40/405303

Cation distribution in nanocrystalline $ZnFe_2O_4$ investigated using x-ray absorption fine structure spectroscopy

M J Akhtar[1,3], M Nadeem[1], S Javaid[1] and M Atif[2]

[1] Physics Division, PINSTECH, PO Nilore, Islamabad, Pakistan
[2] Physics Department, Quaid-i-Azam University, Islamabad, Pakistan

E-mail: javeda@pinstech.org.pk

Received 6 April 2009, in final form 19 August 2009
Published 14 September 2009
Online at stacks.iop.org/JPhysCM/21/405303

Abstract

X-ray absorption fine structure (XAFS) spectroscopy has been employed to investigate the cation distribution in nanocrystalline zinc ferrites ($ZnFe_2O_4$), synthesized in acidic and basic media at different temperatures. By using $(Zn_{1-x}Fe_x)[Ni_xFe_{2-x}]O_4$ as model compounds we have determined cation distribution in nanosize $ZnFe_2O_4$. The cation distribution for samples synthesized at low temperature (400 °C) is $(Zn_{0.5}Fe_{0.5})[Zn_{0.5}Fe_{1.5}]O_4$ for urea- and $(Zn_{0.75}Fe_{0.25})[Zn_{0.25}Fe_{1.75}]O_4$ for citric-acid-based samples. These results show that samples synthesized at and above 600 °C have a local structural environment identical to that of bulk $ZnFe_2O_4$.

(Some figures in this article are in colour only in the electronic version)

1. Introduction

The spinel ferrites have attracted intense global interest in fundamental science such as addressing the relationships between magnetic properties of nanoparticles and their crystal structure. The reason for this interest is the unusual and technologically desirable magnetic properties of these nanomaterials when compared with their bulk counterparts [1, 2]. The relatively high magnetization is explained on the basis of cation distribution between tetrahedral and octahedral sites in the surface region of the ultra-fine particles [3]. The synthesis of materials with new properties by means of the controlled manipulation of their microstructure on the atomic level has become an emerging interdisciplinary field based on solid state physics, chemistry, biology and materials science.

Among spinel ferrites, $ZnFe_2O_4$ is of interest not only to basic research in magnetism, but also has great potential in technological applications. $ZnFe_2O_4$ in bulk form is a normal spinel, where divalent (Zn^{2+}) ions are at the tetrahedral (A) sites and trivalent (Fe^{3+}) ions occupy octahedral (B) sites. However, nanocrystalline $ZnFe_2O_4$ shows mixed spinel structure, where Zn^{2+} and Fe^{3+} are distributed over (A) and (B) sites being represented as $(Zn^{2+}_{1-x}Fe^{3+}_x)[Zn^{2+}_xFe^{3+}_{2-x}]O_4$, where x represents the inversion parameter and corresponds to the degree of cation distribution, i.e., Fe^{3+} ions occupying (A) sites. Figure 1 shows the crystal structure of a typical spinel ferrite, where tetrahedral (A) and octahedral (B) sites are shown. It is well known that in bulk $ZnFe_2O_4$ the antiferromagnetic ordering temperature ($T_N = 10$ K) can be raised by increasing the Fe^{3+} occupation at the tetrahedral sites. This increase of magnetization originates in the stronger inter-sub-lattice (A–B) superexchange interaction as compared to intra-sub-lattice (A–A and B–B) interactions. The ferromagnetic or cluster-glass behaviour of $ZnFe_2O_4$ having a Curie temperature close to 600 K has been reported [4]. Several methods have been employed to synthesize $ZnFe_2O_4$ nanoparticles, including ball milling, coprecipitation, aerogel and hydrothermal methods [5–7]. The magnetic properties are strongly influenced by the composition and microstructure of the particles, which are sensitive to the preparation methodology [8, 9].

The transition temperature (T_N) for most ferrites decreases as the particle size decreases: however, $ZnFe_2O_4$ shows the opposite trend. The origin of this increase has been variously attributed to oxygen vacancies and disorder [10],

[3] Author to whom any correspondence should be addressed.

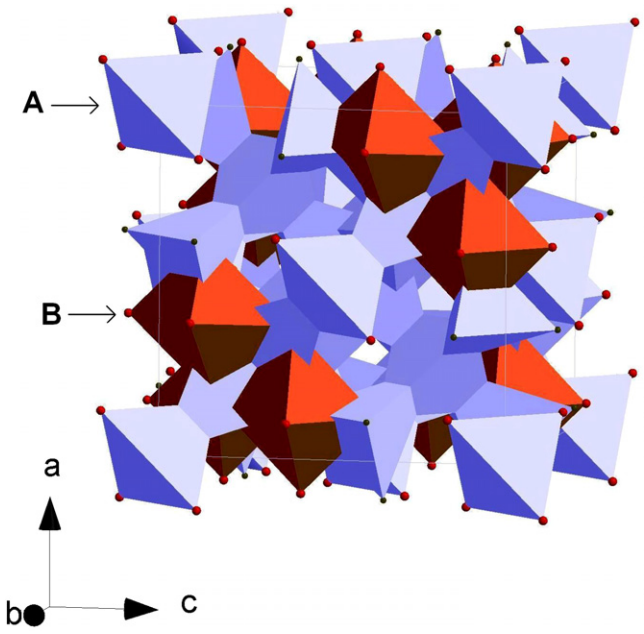

Figure 1. The crystal structure of a typical spinel ferrite (MFe_2O_4), where M is a divalent cation; both tetrahedral (A) and octahedral (B) sites are shown. In a normal spinal ($ZnFe_2O_4$) all Zn are at A sites and all Fe are at B sites, in inverse spinel ($NiFe_2O_4$) all Ni are at B sites and Fe are equally distributed at A and B sites, whereas in mixed spinel (nanosized $ZnFe_2O_4$) Zn and Fe are distributed at both A and B sites, which indicates the degree of inversion.

surface effects [11] and redistribution of Zn or Fe ions at tetrahedral (A) and octahedral (B) sites [12]. A number of studies have been carried out to explain the structural variation due to a decrease in particle size. These include: x-ray and neutron diffraction [5, 13], Mössbauer spectroscopy [11, 14, 15] and x-ray absorption fine structure (XAFS) spectroscopy [16–21].

XAFS spectroscopy has revealed itself as a powerful technique for structural characterization of the local atomic environment of individual atomic species, including bond distances, coordination numbers and type of nearest neighbours surrounding the central atom. This technique is particularly useful for materials that show considerable structural and chemical disorder. Previously a number of XAFS studies have been carried out to investigate the local structural environment of nanocrystalline $ZnFe_2O_4$. Jeyadevan *et al* [17] showed that the local structure of Zn atom is different in bulk and coprecipitated $ZnFe_2O_4$; in the latter case, the structure is distorted due to cation distribution. Oliver *et al* [18] observed variation in the local structure around Zn but not around Fe and found a nonequilibrium distribution of Zn and Fe cations, suggesting overpopulation at octahedral sites. More recently, Stewart *et al* [19] and Nakashima *et al* [20] employed XAFS spectroscopy and used theoretical models to explain the inversion in nanosized $ZnFe_2O_4$. Although these calculations can simulate the XANES features which are comparable to experimental XANES modulations, however, from these calculations precise XANES spectra with variable degrees of inversion are difficult to generate. XAFS spectroscopy has been employed to determine the cation distribution in nanocrystalline $CuFe_2O_4$ and $NiFe_2O_4$ systems [22, 23]. The local structural environment of nanoparticles can be explained on the basis of core and shell, where the core has bulk characteristics but the structure of the shell (surface) is different due to variation in the oxygen coordination numbers in the nearest-neighbour shell [24]. Therefore, in the case of $ZnFe_2O_4$ nanostructure, there is a need to address the surface phenomena as well. In the present study we use $Zn_{1-x}Ni_xFe_2O_4$ as model compounds with known cation distributions to determine the degree of inversion in nanocrystalline $ZnFe_2O_4$. In addition, by using model compounds, which are polycrystalline, we can make a comparative study of surface effects on the local environment of nanocrystalline materials.

It is well known that $NiFe_2O_4$ has an inverse spinel structure with Ni^{2+} ions substituted at B sites and Fe^{3+} ions equally distributed at A and B sites. As discussed earlier, the bulk $ZnFe_2O_4$ has a normal spinel structure, with Zn^{2+} ions at A sites and all Fe^{3+} ions at B sites. Therefore, when Zn^{2+} is substituted with Ni^{2+} in $Zn_{1-x}Ni_xFe_2O_4$, mixed spinel structures having a variable degree of inversion can be obtained. The cation distribution can be represented as $(Zn_{1-x}Fe_x)[Ni_xFe_{2-x}]O_4$, where ( ) and [ ] are used for tetrahedral and octahedral sites, respectively. By comparing the XANES spectra of $Zn_{1-x}Ni_xFe_2O_4$ with nanocrystalline $ZnFe_2O_4$ we can accurately determine the degree of inversion.

2. Experimental details

Nanoparticles of $ZnFe_2O_4$ were prepared by the sol–gel method in two different precursors. The chemical reagents used in the preparation are $Zn(NO_3)_2{\cdot}6H_2O$, $Fe(NO_3)_3{\cdot}9H_2O$, urea and citric acid. All the chemicals are analytical grade. 0.2 M (50 ml) of iron nitrate solution and 0.1 M (50 ml) of zinc nitrate solution have been used and were gelated by using 0.1 M (300 ml) of urea solution as a catalyst and distilled water as the solvent. These solutions were heated to a temperature of 70 °C with vigorous stirring until the gel was formed, which was subsequently dried at 100 °C in an oven. The nanocrystalline $ZnFe_2O_4$ materials were obtained by heating the dried gel in a muffle furnace at temperatures (400, 600 and 800 °C). For the preparation of $ZnFe_2O_4$ nanoparticles in an acidic medium, citric acid was used instead of urea and the rest of the preparation method was the same as described for urea-based samples; further details are given elsewhere [8].

The bulk $Zn_{1-x}Ni_xFe_2O_4$ (where $x = 0.0$–1.0) were synthesized by solid state reaction methods by mixing the appropriate amount of ZnO, Fe_2O_3 and NiO (all having 99.99% purity). Acetone was added to the mixture of these powders, which was finely ground in an electric grinder for 30 min. The powders were heated at 900 °C for 15 h in alumina boats, then cooled to room temperature, reground and heated at 1100 °C for 15 h. The mixture was heated at 1250 °C for 15 h twice. The reaction products were furnace-cooled to room temperature and reground after each heating cycle. Powder x-ray diffraction (XRD) measurements were carried out to confirm that single-phase materials have been prepared.

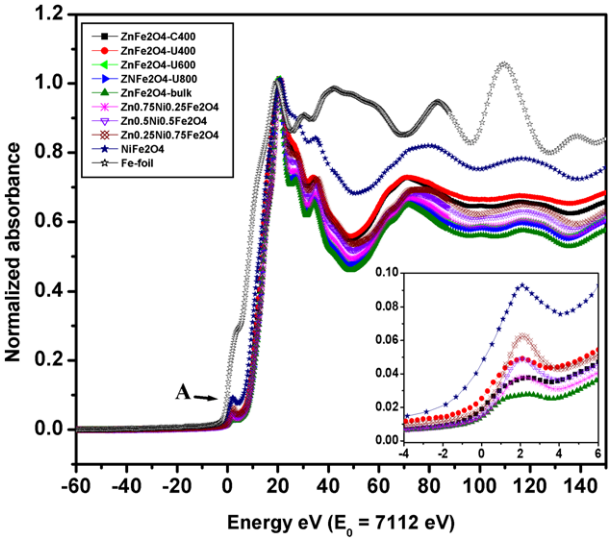

Figure 2. Comparison of the XANES spectra of Fe K-edge in nanocrystalline $ZnFe_2O_4$ and $Zn_{1-x}Ni_xFe_2O_4$. The inset shows zoom of the pre-edge peak in some selected materials.

The XAFS data for the K-edges of Fe (7112 eV) and Zn (9569 eV) were collected at beamline 11.1 (XAFS) at the ELETTRA Synchrotron, Trieste, Italy, with the storage ring running at 2 GeV and a typical current of 200 mA. These data were collected at room temperature and in the transmission mode using an Si(111) monochromator. The Fe and Zn metal foils were used for energy calibration and to check the stability of the beamline and optics system. The samples were prepared by deposition from a powder suspension in cyclohexane on a Millipore membrane (type GS 0.22 μm). Multi-scanned spectra of each sample were collected (2–5 scans) to get a sufficiently high signal-to-noise ratio; these data were merged together in the first step of the analysis.

The XAFS data were processed by using the Daresbury data analysis programs EXBACK and EXCURV92 [25, 26]. EXCURV92 employs full curved wave theory [27] and includes routines to treat multiple scattering effects in highly symmetric structures. Phase shifts were derived within the program from *ab initio* calculations using Hedin–Lundqvist potentials and von Barth ground states. For each spectrum a theoretical model was achieved by adding shells around the central excited atom and least-squares iterating the Fermi energy (E_0), the radial distances (RD) and the Debye–Waller type factors (DWF). Although the coordination numbers (CN) can be iterated, due to their strong correlation with Debye–Waller type factors [28, 29] in the present study coordination numbers were kept fixed to their preset values. The structural uncertainties for RD and CN are about ± 0.02 Å and $\pm 10\%$, respectively, for nearest neighbours, increasing slightly for distant shells. The errors in the fitted parameters are obtained by statistical methods according to the Error Report of the International XAFS Society Standards and Criteria Committee 2000 (http://www.i-x-s.org/OLD/subcommittee_reports/sc/) and the quality of the fit is measured by an R factor.

3. Results and discussion

In order to compare quantitatively the intensity of absorption features in nanocrystalline $ZnFe_2O_4$ with $Zn_{1-x}Ni_xFe_2O_4$, used as reference models, the XANES (x-ray absorption near-edge structure) spectra were normalized. For the normalization of XANES spectra a standard edge step normalization procedure was employed [30]. The normalized XANES spectra were obtained by subtracting the smooth pre-edge absorption from the experimental spectra and taking the edge jump height as unity; further details of the normalization procedure can be found in [30]. The normalized XANES spectra of the Fe K-edge in nanocrystalline $ZnFe_2O_4$ and bulk $Zn_{1-x}Ni_xFe_2O_4$ ($x = 0.0$–1.0) are shown in figure 2; the data for Fe foil is also shown, which is used for the energy calibration. The interpretations of K-edge XANES features for 3d transition metal oxides are well established [30–33]. A small pre-edge peak (labelled as A) is observed in all spectra, which is due to the 1s to 3d (formally electric dipole forbidden) transition, while the main peak can be attributed to 1s to 4p transitions [31]. In the case of the Fe K-edge, both 1s to 3d quadrupole transitions and 1s to 4p dipole transitions are allowed [32], though the intensity of the quadrupole transition is generally very low. The increase in the intensity of the pre-edge peak has been attributed to the local mixing of 4p and 3d orbitals, which is allowed in the tetrahedral symmetry but forbidden in the octahedral symmetry, due to the presence of inversion symmetry [31]. This argument is supported by the DOS calculations where it has been shown that a peak at $\sim$2 eV is due to the e_g level of tetrahedral (A) sites [34]. We observe that the samples synthesized at 600 and 800 °C (both in urea and citric acid) have identical XANES modulations and are close to that of bulk $ZnFe_2O_4$. Therefore, we do not show XANES spectra of samples synthesized in citric acid at 600 and 800 °C. From these data we note that the intensity of the pre-edge peak for 400 °C synthesized samples differs considerably, depending on whether the sample is synthesized in urea or citric acid. Previous studies have shown that in spinel ferrites the intensity of the pre-edge peak increases, when there is an increase in the occupancies of Fe^{3+} at the tetrahedral sites [18, 35]. We use this pre-edge peak to determine the degree of inversion in nanocrystalline $ZnFe_2O_4$ synthesized under different conditions.

The inset of figure 2 shows the blown-up portion of the pre-edge peak in nanocrystalline $ZnFe_2O_4$ synthesized at 400 °C in urea and citric acid along with selected compositions of the $Zn_{1-x}Ni_xFe_2O_4$ series which are used as reference models having known degrees of inversion. From these results we observe that the intensity of the pre-edge peak increases as the concentration of Ni is increased in $Zn_{1-x}Ni_xFe_2O_4$. This is due to the fact that Ni prefers to go to octahedral (B) sites; therefore the same amount of Fe moves to tetrahedral (A) sites. When we compare nanocrystalline $ZnFe_2O_4$ with the bulk $Zn_{1-x}Ni_xFe_2O_4$ series we observe that material synthesized at 400 °C in urea has the same pre-edge peak intensity as that of $(Zn_{0.5}Fe_{0.5})[Ni_{0.5}Fe_{1.5}]O_4$. Therefore the degree of inversion in this material can be represented as $(Zn_{0.5}Fe_{0.5})[Zn_{0.5}Fe_{1.5}]O_4$. For the sample synthesized at

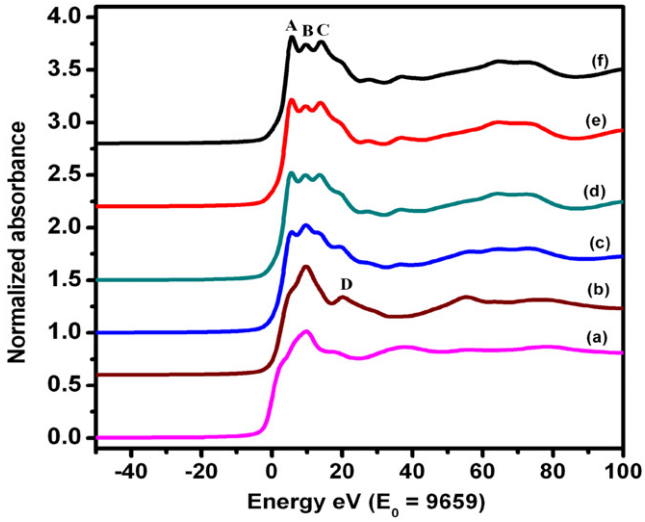

Figure 3. Comparison of the XANES spectra of Zn K-edge in (a) Zn foil, (b) urea-400, (c) citric-400, (d) urea-600, (e) urea-800 and (f) bulk $ZnFe_2O_4$.

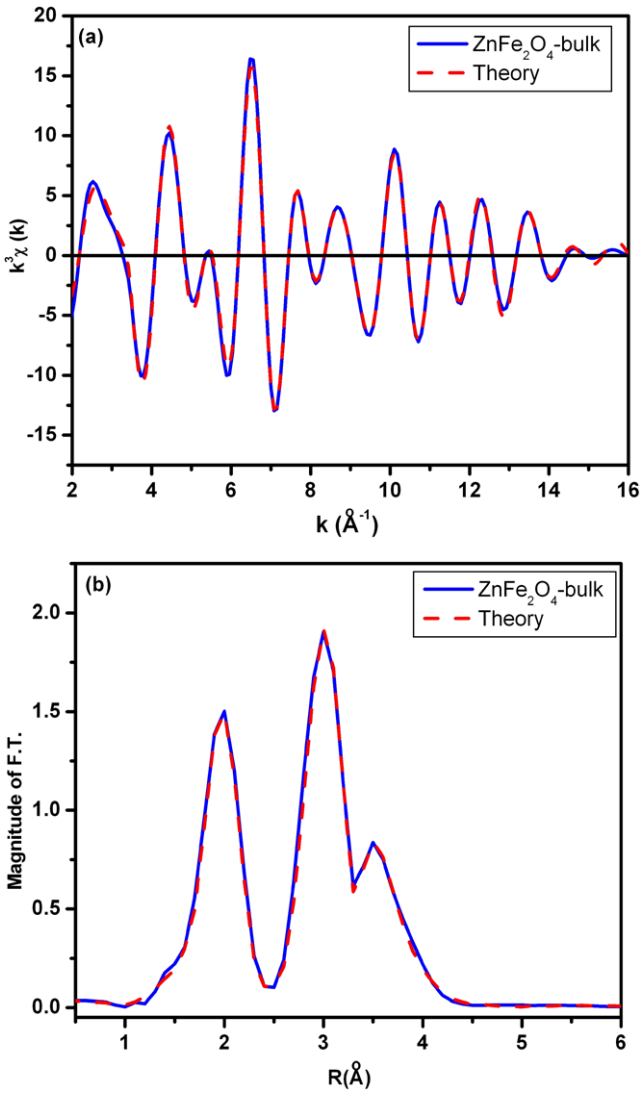

Figure 4. EXAFS spectra (a) and Fourier transform (b) of Fe K-edge in bulk $ZnFe_2O_4$, compared with theoretical model.

400 °C in citric acid the peak height is comparable to that of $(Zn_{0.75}Fe_{0.25})[Ni_{0.25}Fe_{1.75}]O_4$, indicating that in this material inversion corresponds to $(Zn_{0.75}Fe_{0.25})[Zn_{0.25}Fe_{1.75}]O_4$. The peaks for nanocrystalline $ZnFe_2O_4$ are relatively broader compared to the model compounds (which are polycrystalline). This may be due to the surface effects in nanocrystalline materials; we will determine it later in the EXAFS discussion. The intensity of the pre-edge peak for bulk $ZnFe_2O_4$ is smaller than those two compositions, while $Zn_{0.25}Ni_{0.75}Fe_2O_4$ and pure $NiFe_2O_4$ have high pre-edge peak intensities. The present results clearly demonstrate that, by employing $Zn_{1-x}Ni_xFe_2O_4$ as models for mixed spinel structures, we can precisely determine the degree of inversion in nanocrystalline $ZnFe_2O_4$. From these results we can infer that $ZnFe_2O_4$ nanoparticles synthesized in urea at 400 °C have more inversion compared to the material synthesized in citric acid at the same temperature. However, samples synthesized at and above 600 °C have a local structural environment identical to that of bulk $ZnFe_2O_4$ and are independent of the precursor media, acidic or basic.

The normalized XANES spectra of the Zn K-edge in nanocrystalline $ZnFe_2O_4$ prepared at different temperatures (400, 600 and 800 °C) in urea and 400 °C in citric acid are shown in figure 3. As mentioned earlier samples synthesized above 600 °C do not show any variation between urea and citric acid; therefore, samples prepared in citric acid at 600 and 800 °C are not shown here. The data for bulk $ZnFe_2O_4$ (synthesized by the solid state method) and Zn foil (which is used for energy calibration) are also shown. Since Zn in $Zn_{1-x}Ni_xFe_2O_4$ occupies only tetrahedral sites and Ni alone goes to octahedral sites, therefore the Zn edge of $Zn_{1-x}Ni_xFe_2O_4$ cannot be used as a reference model for the determination of inversion parameters in nanocrystalline $ZnFe_2O_4$. In the XANES spectra of the Zn K-edge, there are three main peaks which are labelled as A, B and C. We note that peak B is the main peak in the Zn foil and urea-400 samples and the two shoulder peaks (A and C) are not yet developed. These peaks start to grow in the citric-400 sample, but the central peak (B) is still dominant. However, for samples synthesized at 600 and 800 °C, these shoulder peaks become dominant and the central peak is suppressed, which is comparable to bulk $ZnFe_2O_4$. The present results show that nanoparticles synthesized at 600 °C or above show near-edge structure identical to that of the bulk material, whereas for samples synthesized at 400 °C, the Zn spectra depend on whether an acidic or basic medium is used. We note that for the 400 °C urea-based sample having $(Zn_{0.5}Fe_{0.5})[Zn_{0.5}Fe_{1.5}]O_4$ composition, when Zn ions are 50% distributed at both A and B sites the main central peak is dominant and two shoulder peaks are not developed. However when the sample is synthesized in citric acid at 400 °C, having $(Zn_{0.75}Fe_{0.25})[Zn_{0.25}Fe_{1.75}]O_4$ composition, 3/4 Zn ions are at tetrahedral sites and only 1/4 Zn ions are at octahedral sites, which results in the growth of the shoulder peaks and suppression of the central peak. A peak (marked as D in spectrum (b) of figure 3) ∼20 eV above the edge is prominent in $(Zn_{0.5}Fe_{0.5})[Zn_{0.5}Fe_{1.5}]O_4$ (urea 400 °C

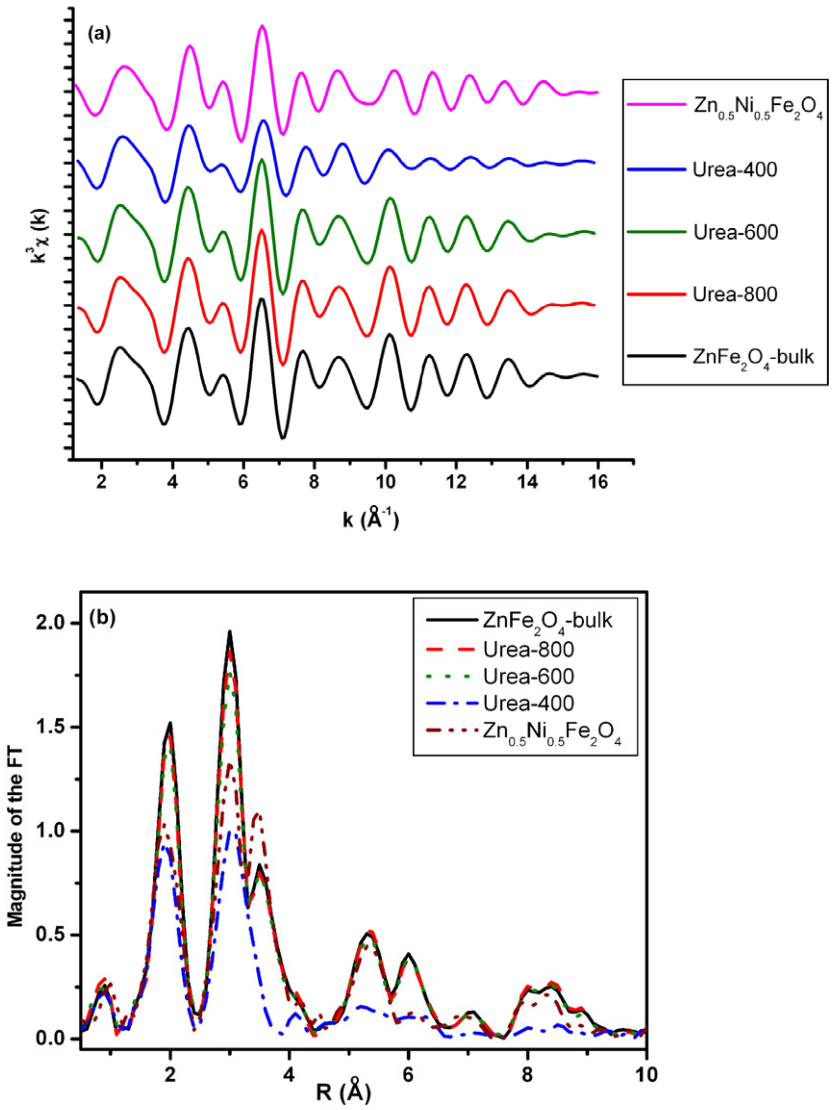

Figure 5. Fe K-edge EXAFS spectra (a) and Fourier transforms (b) in urea-based $ZnFe_2O_4$, along with bulk $ZnFe_2O_4$ and $Zn_{0.5}Ni_{0.5}Fe_2O_4$.

synthesized sample), which is identical to what was observed in ZnO and has been attributed to a phase transition [36]. A similar peak has been observed in the simulated spectrum when an isolated Zn atom is substituted for Fe at B sites in $ZnFe_2O_4$ [18]. However, we note that the simulated peak position is ∼3 eV higher than our experimental value. The difference in the peak positions could be due to the fact that in simulation an isolated Zn atom is substituted at Fe sites. From our experimental data we observe that the intensity of this peak gradually decreases as the concentration of Zn at (B) sites decreases; therefore we can infer that this peak has contributions from Zn^{2+} ions occupying the octahedral sites in nanocrystalline $ZnFe_2O_4$.

EXAFS spectra and Fourier transforms (both experimental and fitted models) of the Fe K-edge in $ZnFe_2O_4$ are shown in figure 4 (to compare with the theoretical model the data are Fourier-filtered). The results obtained from the best fitted model are presented in table 1. These results are in good agreement with the bond lengths obtained from the lattice parameters [37]. For the Fe edge, we note that there is one peak at ∼2.0 Å which is due to the first shell of oxygen atoms, the second peak at ∼3.0 Å is due to Fe second-nearest neighbours, while the third peak at ∼3.5 Å is due to the combination of Zn and oxygen atoms. The theoretical model presented in table 1 can be fitted to nanocrystalline $ZnFe_2O_4$ synthesized at 600 and 800 °C (only the results for samples synthesized at 800 °C are presented). The

Table 1. Radial distribution of Fe K-edge in $ZnFe_2O_4$.

		Bulk $ZnFe_2O_4$		Urea-800	
Shell	CN	RD (Å)	DWF (Å^2)	RD (Å)	DWF (Å^2)
Fe–O	6.0	2.02 ± 1	0.010 ± 1	2.01 ± 1	0.011 ± 1
Fe–Fe	6.0	2.99 ± 1	0.010 ± 1	2.99 ± 1	0.011 ± 1
Fe–O	2.0	3.47 ± 2	0.004 ± 3	3.48 ± 2	0.004 ± 3
Fe–Zn	6.0	3.51 ± 3	0.019 ± 4	3.52 ± 1	0.020 ± 3
Fe–O	6.0	3.61 ± 2	0.018 ± 9	3.60 ± 3	0.038 ± 7
		R factor = 10.11%		R factor = 10.23%	

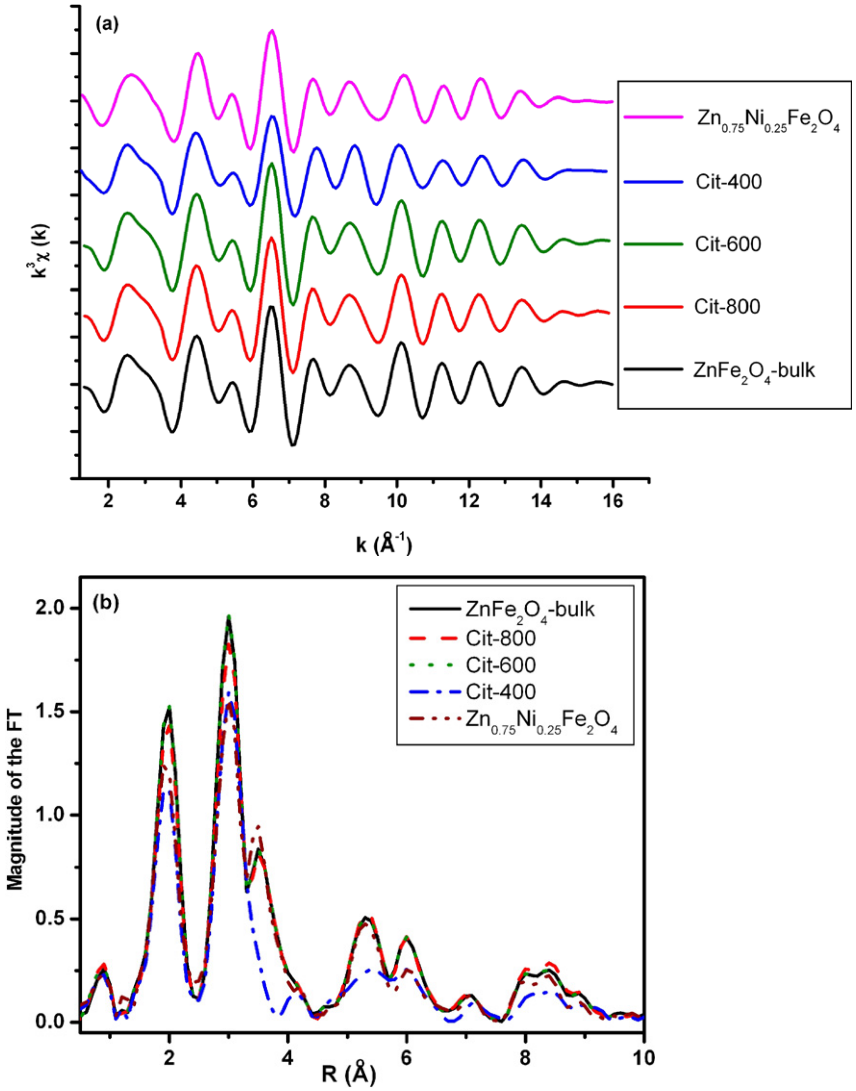

Figure 6. Fe K-edge EXAFS spectra (a) and Fourier transforms (b) in citric-acid-based $ZnFe_2O_4$, along with bulk $ZnFe_2O_4$ and $Zn_{0.75}Ni_{0.25}Fe_2O_4$.

EXAFS spectra and Fourier transforms of the Fe K-edge for $ZnFe_2O_4$ (bulk and nanoparticles prepared in urea at different temperatures) along with $Zn_{0.5}Ni_{0.5}Fe_2O_4$ are shown in figure 5. We note that in the case of the urea-400 sample the EXAFS amplitude reduces significantly at higher k space (figure 5(a)). Since in EXAFS the amplitude is proportional to the coordination number, therefore these results show that coordination numbers reduce in the case of nanocrystalline $ZnFe_2O_4$, suggesting loss of long range order. When we look at the Fourier transforms it is evident that the intensity of the first peak is reduced in 400 °C synthesized samples; in addition, the second and third peaks are not resolved. We observe that both peaks have low peak intensities in the urea 400 °C sample, $(Zn_{0.5}Fe_{0.5})[Zn_{0.5}Fe_{1.5}]O_4$ (figure 5(b)). The intensity of the first peak (which is due to first-shell oxygen atoms) is comparable with that of the model compound ($Zn_{0.5}Ni_{0.5}Fe_2O_4$), clearly indicating that the degree of inversion is the same in both samples. However, the EXAFS oscillation in $Zn_{0.5}Ni_{0.5}Fe_2O_4$ is similar to bulk material even at higher k space. From these results we note that in the case of the urea-400 sample the surface effects are significant and in addition to inversion there is no long range order present in this material. These effects are also observed in the Fourier-transform spectra where the magnitude of the Fourier transform is reduced considerably after 4.0 Å for the urea-400 sample.

Figure 6 shows the comparison of EXAFS spectra and Fourier transforms of nanocrystalline $ZnFe_2O_4$ synthesized in citric acid along with bulk $ZnFe_2O_4$ and $Zn_{0.75}Ni_{0.25}Fe_2O_4$. Here we again note that the intensity of the first peak is reduced in the citric-400 sample compared to the other samples, although the EXAFS oscillations (figure 6(a)) are low, but not as much as was observed in the urea-400 sample. From the Fourier transforms it is observed that the intensity of the first peak in the citric-400 sample is reduced (figure 6(b)) when compared with bulk $ZnFe_2O_4$ and high temperature synthesized samples. When these peaks are compared with $Zn_{0.75}Ni_{0.25}Fe_2O_4$, we note there is good

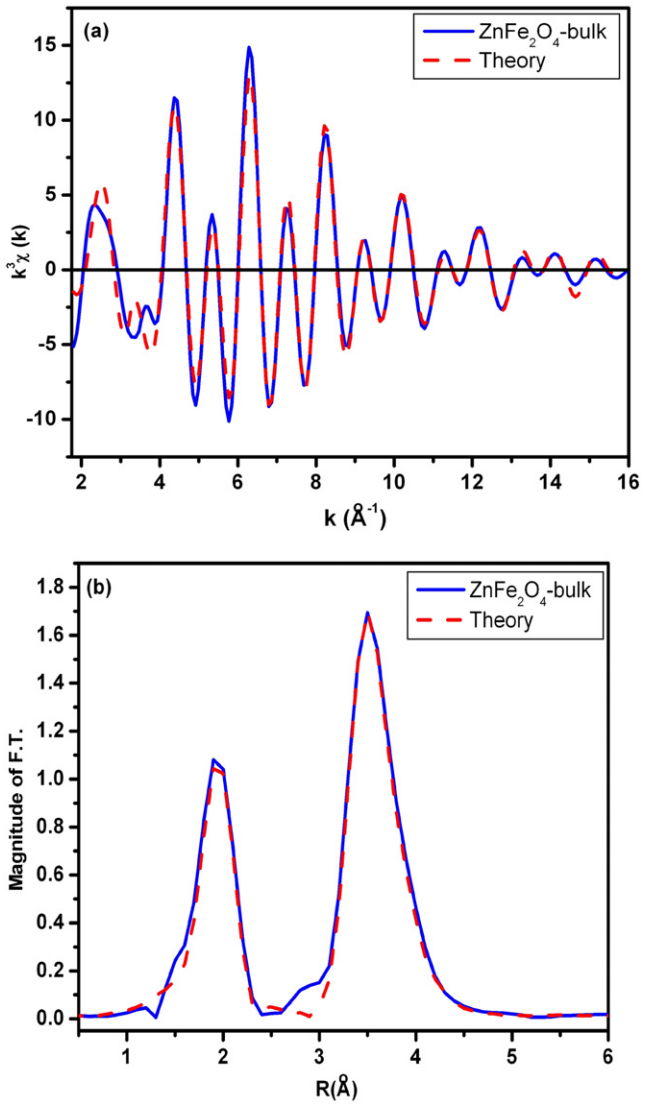

Figure 7. EXAFS spectra (a) and Fourier transform (b) of Zn K-edge in bulk $ZnFe_2O_4$, compared with theoretical model.

agreement between the two peaks. From these results we can deduce that the sample synthesized in citric acid at 400 °C has inversion of $(Zn_{0.75}Fe_{0.25})[Zn_{0.25}Fe_{1.75}]O_4$. For the citric-400 sample we also note that the magnitude of the Fourier transform is relatively low after 4.0 Å compared to the $Zn_{0.75}Ni_{0.25}Fe_2O_4$ which can be inferred from the surface effects in nanocrystalline materials.

The results of Fe K-edge EXAFS data analysis show that there is no considerable change in the local environment of nanocrystalline materials when synthesized at and above 600 °C, compared with bulk $ZnFe_2O_4$. However, from these results we observe that when $ZnFe_2O_4$ is synthesized at low temperature (400 °C) there is a local structural change around Fe, which arises due to different degrees of inversion and surface effects in nanocrystalline $ZnFe_2O_4$. It is clear from these findings that $ZnFe_2O_4$ nanoparticles having various degrees of inversion can be obtained by applying different synthesis conditions.

Table 2. Radial distribution of Zn K-edge in $ZnFe_2O_4$.

		Bulk $ZnFe_2O_4$		Urea-800	
Shell	CN	RD (Å)	DWF (Å^2)	RD (Å)	DWF (Å^2)
Zn–O	4.0	1.98 ± 1	0.009 ± 1	1.98 ± 1	0.009 ± 1
Zn–Fe	12.0	3.51 ± 2	0.015 ± 2	3.52 ± 1	0.014 ± 2
Zn–O	12.0	3.53 ± 3	0.031 ± 4	3.53 ± 2	0.026 ± 5
Zn–Zn	4.0	3.65 ± 2	0.014 ± 2	3.66 ± 2	0.014 ± 2
		R factor = 22.59%		R factor = 23.52%	

In figure 7 EXAFS spectra and Fourier transforms (both experimental and fitted model) of the Zn K-edge in bulk $ZnFe_2O_4$ are shown (to compare with the theoretical model the data are Fourier-filtered). The results obtained from the best fit are presented in table 2: for comparison, data obtained from nanoparticles synthesized in urea at 800 °C is also given. For nanocrystalline materials synthesized at 600 and 800 °C this model can be fitted; we do not observe any appreciable change between the local structural environments of nanoparticles and bulk $ZnFe_2O_4$. The EXAFS spectra and Fourier transforms of Zn K-edge in nanocrystalline $ZnFe_2O_4$, prepared at different temperatures, in urea and citric acid along with the bulk sample are shown in figure 8. We note that the amplitude, frequency and phase of the EXAFS spectrum of the urea 400 °C synthesized sample are different from $Zn_{0.5}Ni_{0.5}Fe_2O_4$ and bulk $ZnFe_2O_4$ spectra (figure 8(a)). This is due to the fact that in $Zn_{0.5}Ni_{0.5}Fe_2O_4$ all Zn are at A sites (as in the case of bulk $ZnFe_2O_4$), whereas in the urea-400 sample Zn are distributed at both A and B sites having $(Zn_{0.5}Fe_{0.5})[Zn_{0.5}Fe_{1.5}]O_4$ composition. The phase and amplitude of the EXAFS provide information about the type of scattering atoms [38]; which are different when Zn is at a tetrahedral site or occupies an octahedral site, having inversion symmetry. This clearly shows that the Zn K-edge in $Zn_{0.5}Ni_{0.5}Fe_2O_4$ cannot be used as a model for the determination of local environment around Zn in $ZnFe_2O_4$ nanocrystalline materials. From Fourier transforms (figures 8(b) and (c)) we observe that for all samples there is not much difference in the intensity of the first peak. However, we note that for samples synthesized at 400 °C, the amplitude of the second peak decreases considerably; furthermore, in the case of the urea-400 sample, $(Zn_{0.5}Fe_{0.5})[Zn_{0.5}Fe_{1.5}]O_4$, there is a shift in the peak position towards lower radial distance. This can be expected, because when Zn moves from tetrahedral to octahedral sites the second-nearest neighbour distance decreases ∼3.5 to ∼3.0 Å and the number of second-nearest neighbours reduces from 12 to 6. For materials synthesized at 400 °C in citric acid, $(Zn_{0.75}Fe_{0.25})[Zn_{0.25}Fe_{1.75}]O_4$, the structural changes are less prominent, because 3/4 Zn atoms are at tetrahedral sites and only 1/4 Zn atoms occupy the octahedral symmetry. From these results we can infer that contributions from second-nearest neighbours vary in nanocrystalline $ZnFe_2O_4$, where tetrahedral symmetry is considerably different from the octahedral symmetry.

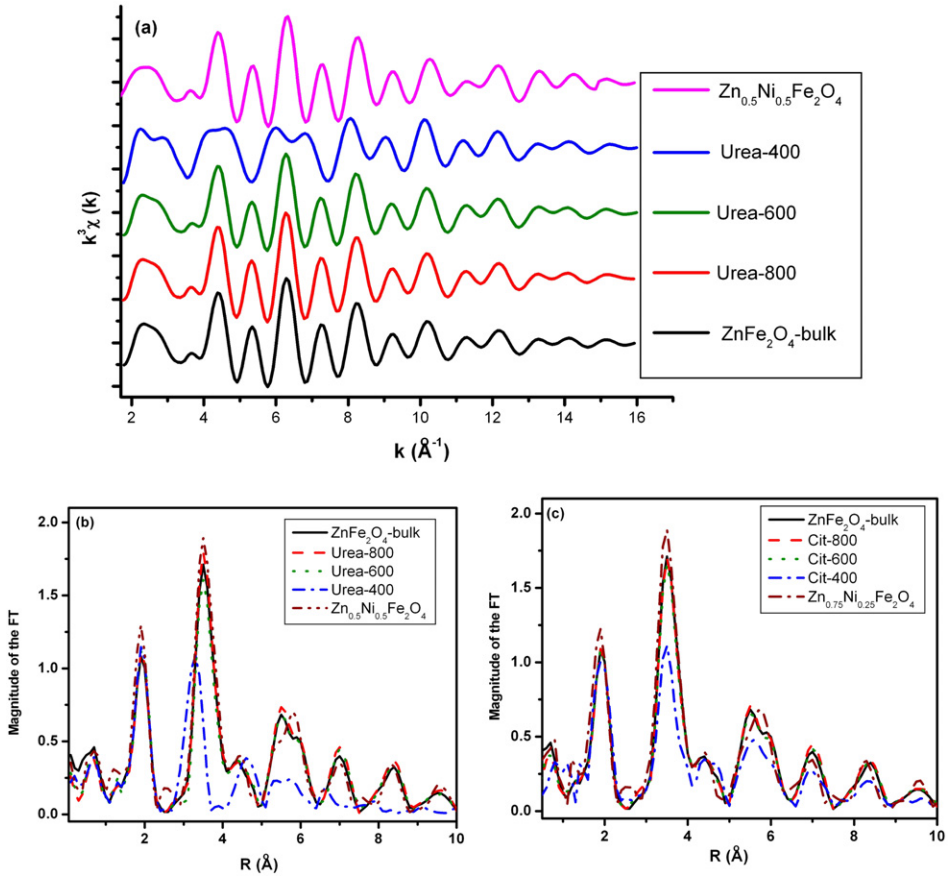

Figure 8. Zn K-edge EXAFS spectra (a) and Fourier transforms (b) of urea-based $ZnFe_2O_4$, along with bulk $ZnFe_2O_4$ and $Zn_{0.5}Ni_{0.5}Fe_2O_4$ and Fourier transforms of citric acid based $ZnFe_2O_4$, along with bulk $ZnFe_2O_4$ and $Zn_{0.75}Ni_{0.25}Fe_2O_4$ (c).

4. Conclusion

From the above results we can conclude that by employing XAFS spectroscopy we can precisely determine the cation distribution in nanocrystalline $ZnFe_2O_4$, using $Zn_{1-x}Ni_xFe_2O_4$ as model compounds. We found that for samples synthesized at low temperature (400 °C) the degree of inversion depends on the precursor medium. For urea-based samples the degree of inversion is found to be $(Zn_{0.5}Fe_{0.5})[Zn_{0.5}Fe_{1.5}]O_4$, whereas for materials synthesized at 400 °C in citric acid, the cation distribution is $(Zn_{0.75}Fe_{0.25})[Zn_{0.25}Fe_{1.75}]O_4$. However, materials synthesized at 600 °C and above have a local structural environment identical to that of bulk $ZnFe_2O_4$. These results clearly demonstrate that the use of model compounds with known cation distribution can be employed to determine the degree of inversion in nanocrystalline spinel ferrites. In addition, these results show that, apart from inversion, surface effects are prominent in nanocrystalline $ZnFe_2O_4$ synthesized in urea at 400 °C.

Acknowledgments

We acknowledge the support of Elettra Synchrotrone, Trieste, Italy, for the provision of beam time and the ICTP-Elettra users' programme for a financial grant. We are grateful to Dr Luca Olivi for his valuable suggestions and help during XAFS data collection.

References

[1] Gleiter H 2000 *Acta Mater.* **48** 1
[2] Moriarty P 2001 *Rep. Prog. Phys.* **64** 297
[3] van der Zaag P J, Brabers V A M, Johnson M T, Noordermeer A and Bongers P F 1995 *Phys. Rev.* B **51** 12009
[4] Chen Y F, Spoddig D and Ziese M 2008 *J. Phys. D: Appl. Phys.* **41** 205004
[5] Kamiyama T, Haneda K, Sato T, Ikeda S and Asano H 1992 *Solid State Commun.* **81** 563
[6] Ho J C, Hamdeh H H, Chen Y Y, Lin S H, Yao Y D, Willey R J and Oliver S A 1995 *Phys. Rev.* B **52** 10122
[7] Shenoy S D, Joy P A and Anantharaman M R 2004 *J. Magn. Magn. Mater.* **269** 217
[8] Atif M, Hasanain S K and Nadeem M 2006 *Solid State Commun.* **138** 416
[9] Philip J, Gnanaprakash G, Panneerselvam G, Antony M P, Jayakumar T and Raj B 2007 *J. Appl. Phys.* **102** 054305
[10] Goya G F and Rechenberg H R 1999 *J. Magn. Magn. Mater.* **196/197** 191
[11] Li F S, Wang L, Wang J B, Zhou Q G, Zhou X Z, Kunkel H P and Williams G 2004 *J. Magn. Magn. Mater.* **268** 332
[12] Jayadevan B, Tohji K, Nakatsuka K and Narayanasamy A 2000 *J. Magn. Magn. Mater.* **217** 99
[13] Shimada T, Tachibana T, Nakagawa T and Yamamoto T A 2004 *J. Alloys Compounds* **379** 122

[14] Upadhyay C, Verma H C and Anand S 2004 *J. Appl. Phys.* **95** 5746
[15] Oliver S A, Hamdeh H H and Ho J C 1999 *Phys. Rev.* B **60** 3400
[16] Calvin S, Carpenter E E, Ravel B, Harris V G and Morrison S A 2002 *Phys. Rev.* B **66** 224405
[17] Jeyadevan B, Tohji K and Nakatsuka K 1994 *J. Appl. Phys.* **76** 6325
[18] Oliver S A, Harris V G, Hamdeh H H and Ho J C 2000 *Appl. Phys. Lett.* **76** 2761
[19] Stewart S J, Figueroa S J A, Ramallo López J M, Marchetti S G, Bengoa J F, Prado R J and Requejo F G 2007 *Phys. Rev.* B **75** 073408
[20] Nakashima S, Fujita K, Tanaka K, Hirao K, Yamamoto T and Tanaka I 2007 *Phys. Rev.* B **75** 174443
[21] Henderson C M, Charnock J M and Plant D A 2007 *J. Phys.: Condens. Matter* **19** 076214
[22] Krishnan V, Selvan R K, Augustin C O, Gedanken A and Bertagnolli H 2007 *J. Phys. Chem.* C **111** 16724
[23] Carta D, Loche D, Mountjoy G, Navarra G and Corrias A 2008 *J. Phys. Chem.* C **112** 15623
[24] Wu Z, Zhang J, Chen X, Chen Z, Sun M, Wu Z and Guo L 2005 *Phys. Scr.* T **115** 802
[25] Morrel C, Baines J T M, Campbell J C, Diakun G P, Dobson B R, Greaves G N and Hasanain S S 1988 *SERC Daresbury Laboratory, EXAFS Users Manual*
[26] Stephenson P, Binsted N, Gurman S J and Campbell J W 1992 *SERC Daresbury Laboratory, EXCURV92 Program*
[27] Gurman S J, Binsted N and Ross I 1984 *J. Phys. C: Solid State Phys.* **17** 143
[28] Akhtar Z N, Akhtar M J and Catlow C R A 1994 *J. Mater. Chem.* **4** 1081
[29] Akhtar M J, Shaheen R, Haque M N, Bashir J and Akhter J I 2000 *Supercond. Sci. Technol.* **13** 1612
[30] Wong J, Lyte F W, Messmer R P and Maylotte D H 1984 *Phys. Rev.* B **30** 5596
[31] Groot de F 2001 *Chem. Rev.* **101** 1779
[32] Westre T E, Kennepohl P, DeWitt J G, Hedman B, Hodgson K O and Solomon E I 1997 *J. Am. Chem. Soc.* **119** 6297
[33] Chaurand P, Rose J, Briois V, Salome M, Proux O, Nassif V, Olivi L, Susini J, Hazemann J L and Bottero J Y 2007 *J. Phys. Chem.* B **111** 5101
[34] Anisimov V I, Elfimov I S, Hamada N and Terakura K 1996 *Phys. Rev.* B **54** 4387
[35] Bonsdorf G, Denecke M A, Schafer K, Christen S, Langbein H and Gunber W 1997 *Solid State Ion.* **101–103** 351
[36] Liu H, Yang J, Zhang Y, Yang L, Wei M and Ding X 2009 *J. Phys.: Condens. Matter* **21** 145803
[37] Schiessl W, Potzel W, Karzel H, Steiner M, Kalvius G M, Martin A, Krause M K, Halevy I, Gal J, Schafer W, Will G, Hillberg M and Wappling R 1996 *Phys. Rev.* B **53** 9143
[38] Penner-Hahn J E 1999 *Coord. Chem. Rev.* **190–192** 1101